

Impact of Background Radiation on the Long Wave Infrared Radiation Characteristics of Aircraft at High Altitude

Wei Huang^{#,*} and Hong-hu Ji[#]

[#]Jiangsu Province Key Laboratory of Aerospace Power System,
Nanjing University of Aeronautics and Astronautics, Nanjing-210 016, China
^{*}E-mail: hw_one@163.com

ABSTRACT

Reflected background infrared radiation is an important contributor to the aircraft total infrared radiation. A reverse Monte Carlo ray tracing method to compute the infrared radiation signature of aircraft was introduced. The impact of atmospheric and ground radiation on the long wave infrared radiation signature of aircraft at the altitude of 11 km is analysed. The flight speed is Mach 0.8. The horizontal detection directions, downward detection directions and upward detection directions are considered. The results show that in the horizontal plane, the ratio of reflected background infrared radiation to self infrared radiation is about 10 per cent in summer, and 7 per cent in winter; the ratio values distributed in the front and side of the aircraft are bigger than that in the rear; and the existence of atmospheric and ground infrared radiation makes the apparent radiance temperature of the lower part of the aircraft higher than that of the upper part of the aircraft.

Keywords: Infrared radiation, aircraft, high altitude, infrared radiation signature

1. INTRODUCTION

The infrared radiation (IR) signature of the aircraft has a wide range of applications, especially in defence science. The infrared energy emitted from aircraft is a good target to detect and track. Fighter planes even at high altitude is becoming easy target for air-to-air missiles¹. For long range detection, the airborne infrared search and track system which is working in long wave (8 μm ~ 14 μm) is the main anti-aircraft threat. In general, the IR signature of an aircraft is attributed to the main sources: wall emission of skin and engine hot parts, the hot plume, the reflected background by the skin, and the atmospheric attenuation. In long wave band, the dominant background radiation is atmospheric and earth surface infrared radiation. For the considerations of stealth, the infrared radiation of a new designed or improved aircraft has to be simulated and analysed, in order to reduce the IR signatures².

Mahulikar³, *et al.* proposed a survey study of infrared signature of aerospace vehicles. Some standard models for prediction of IR signature were introduced in their article, such as NIRATAM⁴, SPRITITS⁵, SIRUS⁶, and IRST. There are also other standard models. The SIGGE code⁷⁻⁸, developed by Swedish Defense Research Agency, computes the aircraft signatures and has been validated on the RM12 engine. The large commercial aircraft infrared radiation code, LCAIR⁹, developed by AFIT, computes aircraft intensity at takeoff and landing and has been enhanced by introducing the bidirectional reflectance distribution functions (BRDF) which can reduce the computation errors. The CRIRA^{2,10} Code, developed at ONERA, has been upgraded with a global illumination model and validated on Boeing 737 airplane. These standard analysis

models were made more perfect by experimental validation, so that they can be used in IR simulation.

Rao¹¹, *et al.* investigated the effect of atmospheric transmission and radiance on an aircraft infrared signatures at low altitude of 5 km. The results showed that the atmospheric transmittance and radiance had a significant role in determining infrared signature levels of aircraft in band 8 μm ~ 12 μm . But the effect of earth ground IR was not considered in their investigation. Lu¹², *et al.* investigated the aircraft-skin infrared radiation characteristics, however, the environmental radiation was not considered in the simulation. It seems that in literatures the investigation of the effect of environmental radiation on the IR signature of aircraft is insufficient, especially for a cruise aircraft at high altitude. High altitude environment has an obvious characteristic is that the environmental infrared radiation under the aircraft is far larger than that above the aircraft.

The effect of atmospheric and earth ground IR on the long wave infrared radiation signature of an aircraft at high altitude (e. g. 11 km) is assessed. This study is useful for understanding the IR signature of aircraft and the contribution of individual infrared signature contributor, and reducing the total infrared signature of the aircraft.

2. COMPUTATION METHOD OF AIRCRAFT INFRARED

2.1 Procedure of Aircraft Infrared Radiation Computation

The procedure of aircraft infrared radiation computation is a complex process, which involves geometry modelling, CFD computation domain meshing, CFD computation,

infrared radiation computation, and correction of atmosphere transmittance. The relationship between CFD computation and infrared radiation computation is described by Huang and Ji¹³. The computation was divided into two modules, which are commercial CFD module and IR module, respectively. The essence of aircraft infrared computation is solving the radiation transfer equation, which depends on the temperature and emissivity of wall, the temperature and species concentration distributions of the plume. The temperature and species concentration distributions were obtained by solving the momentum, energy, and species transfer equations by the method of CFD.

2.2 Total Infrared Radiation

The total aircraft infrared radiation including background is showing in Fig. 1. Both the aircraft self IR and reflected IR are included in the total IR. The reflected IR is coming from atmosphere, earth ground and sun. The emphasis of this paper is concerned on the effect of atmosphere and earth ground, the effect of the sun radiation on aircraft signature is not studied in this paper. The computational formula is:

$$I_{\text{total}}(\lambda) = (I_{\text{self}}(\lambda) + I_{\text{reflected}}^{\text{atmosphere}}(\lambda) + I_{\text{reflected}}^{\text{ground}}(\lambda)) \cdot \tau(\lambda) + I_{\text{path}}(\lambda) \quad (1)$$

where $I_{\text{self}}(\lambda)$ (unit: $W/(sr \cdot \mu m)$) is the self IR of aircraft, $I_{\text{reflected}}^{\text{atmosphere}}(\lambda)$ is the reflected atmospheric IR, $I_{\text{reflected}}^{\text{ground}}(\lambda)$ is the reflected ground surface IR, $\tau(\lambda)$ is the transmittance of the media between the aircraft and detector, $I_{\text{path}}(\lambda)$ is path IR due to atmosphere.

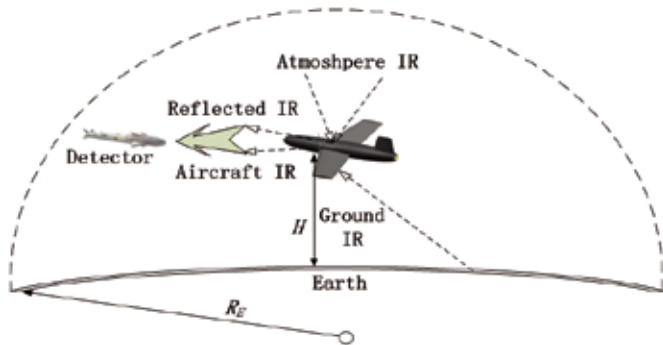


Figure 1. A sketch map of aircraft infrared radiation including background.

The media between the aircraft and detector is assumed to be a non-scattering atmosphere. The MODTRAN code was used to compute the transmittance $\tau(\lambda)$. The transmittance between $8 \mu m$ to $13 \mu m$ is very high, and it is suitable for detection. Two standard atmosphere models, the Mid latitude Summer model and the Mid latitude Winter model, were used to compute atmospheric radiation and absorption.

2.3 Computation of Self Infrared Radiation and Reflected Background Infrared Radiation

Reverse Monte Carlo ray tracing method (RMCM) was applied to compute the aircraft self IR and reflected background

IR. The basic idea of the RMCM is to emit a huge number of rays from the surface of detector in the field of view (FOV), and then tracing the destination of each ray by statistical criterions. To display the thermal figure of the target, the FOV is divided into many individual pixels in direction θ and ϕ , as shown in Fig. 2. The infrared radiance of each pixel is the average value of the rays; and typical ray number in each pixel is 40 or more.

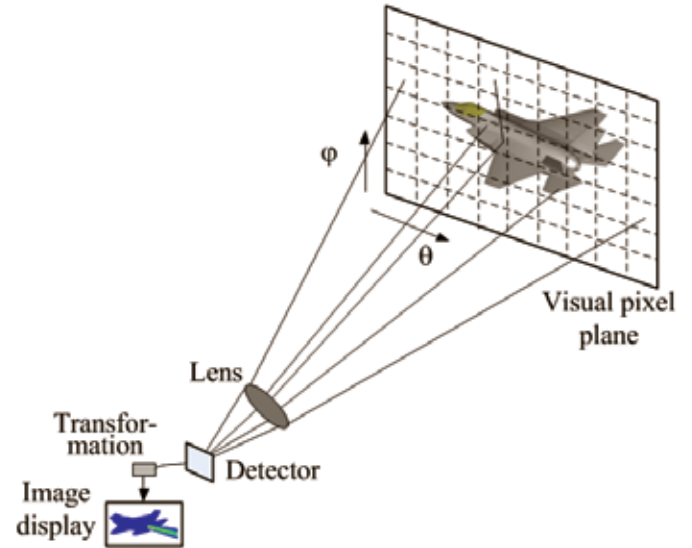


Figure 2. Illustration of infrared image display and reverse Monte Carlo ray tracing.

There are four possible destinations for each ray:

- (i) The ray does not intersect with the aircraft skin or engine plume, and it reaches the surrounded environment.
- (ii) The ray is directly absorbed by the wall or the plume.
- (iii) The ray is reflected by wall, and finally absorbed by the wall or the plume.
- (iv) The ray is reflected by the wall, and finally goes into the surrounded atmosphere or ground.

Once a ray reaches the plume, it will propagate a step of length ds . It is assumed that the ray could either be absorbed by the non-scattering medium or pass through it. The occurrence of each event is related to both the absorptivity, $\alpha_\lambda (= 1 - \tau(\kappa_\lambda, ds))$, and a random number RAN_a generated for this step, where τ is the transmissivity, κ_λ is the absorb coefficient. RAN_a is uniformly distributed between 0 to 1. If RAN_a is larger than α_λ , the ray passes through the medium of the step, and then propagates forward a further step. Otherwise, the ray is absorbed by the medium of the step.

Once a ray reaches the wall, it will either be absorbed or reflected. The occurrences of these events are determined by comparing the emissivity, ϵ_λ of the wall to the random number RAN_e generated for the intersection of the ray and the wall. If RAN_e is smaller than ϵ_λ , the ray is absorbed by the wall, or else the ray is reflected by the wall.

If the ray is absorbed by plume or aircraft wall, the IR energy of local element, where absorption is happened, is carried back to the detector. If the ray is reflected by wall and reaches the surrounded environment, the environment IR energy is carried back to the detector.

The formula of self IR is:

$$I_{\text{self}}(\lambda) = \frac{\Omega_{FOV} R^2}{\pi N} \sum_{i=1}^N E_b(T_i, \lambda) \quad (2)$$

where Ω_{FOV} (sr) is the solid angle of FOV, $R(m^2)$ is the detect range, N is the number of reverse ray, M is the discrete number of waveband, $E_b(W/(m^2 \cdot \mu m))$ is the black body spectral emissive power, T_i is the plume or wall temperature at the position of absorption.

$$E_b(T_i, \lambda) = \frac{c_1 \lambda^{-5}}{\exp[c_2/(\lambda T_i)] - 1} \quad (3)$$

where $c_1 = 3.7418 \times 10^{-16} W \cdot m^2$, $c_2 = 1.4388 \times 104 \mu m \cdot K$.

The formula of reflected background IR is:

$$I_{\text{reflect}}(\lambda) = \frac{(1 - \varepsilon_\lambda) A_{ac}}{\pi} \left[\int_{\mathbf{n}_w \cdot \mathbf{s}_0 < 0} L(\lambda, \theta) |\mathbf{n}_w \cdot \mathbf{s}_0| d\omega_0 + \int_{\mathbf{n}_w \cdot \mathbf{s}_g < 0} \frac{\varepsilon_{ground}}{\pi} E_b(T, \lambda) \tau_{path}(\lambda) |\mathbf{n}_w \cdot \mathbf{s}_g| d\omega_g \right] \quad (4)$$

where \mathbf{n}_w is the normal vector of aircraft wall, \mathbf{s}_0 is the illuminate vector of atmospheric radiance, \mathbf{s}_g is the illuminate vector of ground radiance, $d\omega_0$ is the solid angle of atmosphere radiance, $d\omega_g$ is the solid angle of ground radiance, $L(\lambda, \theta)$ ($W/(m^2 \cdot sr \cdot \mu m)$) is the spectral radiance of atmosphere of zenith angle θ , $\tau_{path}(\lambda)$ is the transmittance of distance between aircraft and ground.

The radiance of the atmosphere at the altitude of 11km is shown in Fig. 3. The radiance was computed by using MODTRAN code. Zenith angle θ defines the path zenith angle at the observer height in degrees. Straight uplook (zenith) paths at 0° ; paths looking to the side (horizon) at 90° ; straight downlook paths (nadir) at 180° . The downlook atmospheric radiance of summer (e.g. $\theta = 135^\circ$) is much bigger than that of winter; but the uplook atmospheric radiance of summer (e.g. $\theta = 45^\circ$) is almost the same as that of winter. The atmospheric radiance is mostly distributing in $8 \mu m \sim 14 \mu m$.

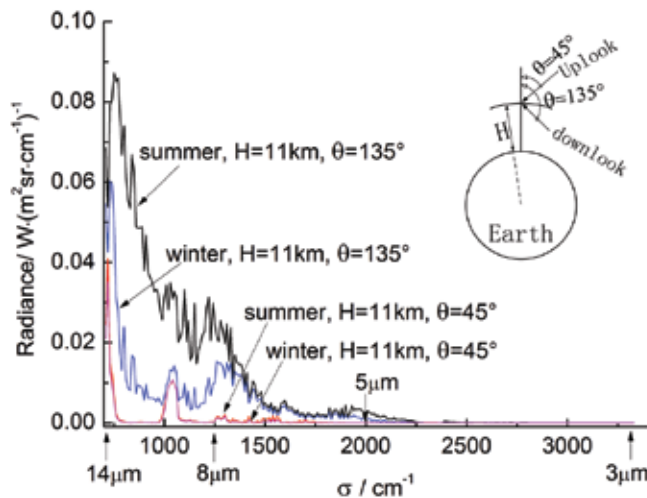


Figure 3. Radiance of the atmosphere at the altitude of 11 km (two atmosphere models, two zenith angles).

2.4 Detection Coordinate System

The infrared radiation signature of the aircraft is related to the detection direction. Figure 4 shows the aircraft IR detection coordinate system, which uses the gravity center of aircraft as the origin. Angle α represents the intersection angle of arbitrarily radiation direction and aircraft axial, at arbitrarily conical plane. Straight nose direction has a value of 0° ; straight rear direction has a value of 180° . Angle β represents the intersection angle of conical plane and horizontal plane. The downward view plane has a positive value; the upward view plane has a negative value.

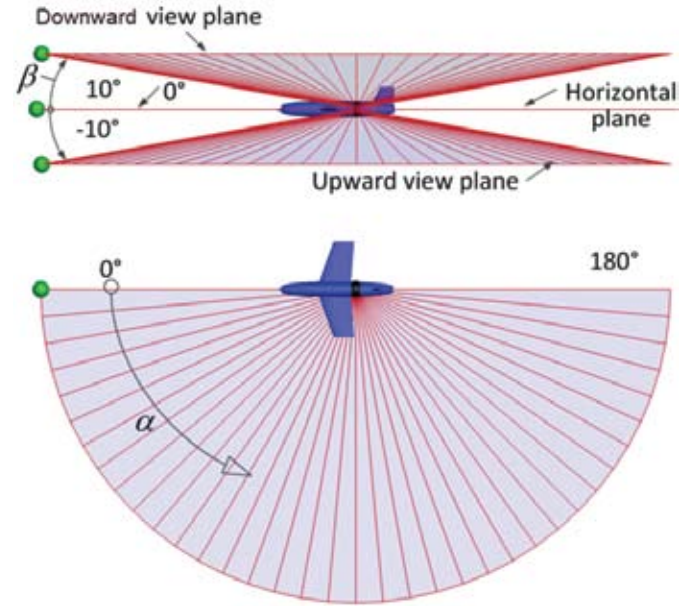


Figure 4. Detection coordinate system.

3. VERIFICATION AND VALIDATION

Verification is defined as a process for assessing simulation numerical uncertainty. Validation is defined as a process for assessing simulation modeling uncertainty. We use an ideal model, which temperature is 800 K and emissivity is 0.8, to verify the computation code is correct. Then, we use a benchmark experimental data tested by Nelsson¹⁴, *et al.* to validate the computation method of aircraft infrared. The experimental data include the self-emission of the wall and the reflection of the environmental infrared radiation and hence it can be used to validate computation method. The long wave radiance of two different panels, one is dark green paint (emissivity is 0.8 and temperature is $32^\circ C$) and the other is dark green foil (emissivity is 0.4 and temperature is $36^\circ C$), was tested by a THV900 camera with filter $7.5 \mu m \sim 12 \mu m$.

Figure 5 shows the comparison of computation and theory results. Compared to theory results, the max error of computation is less 0.6 per cent, which indicates that the computation code is correct and has enough accuracy.

Table 1 shows the comparison with the calculated apparent infrared radiance and the measured apparent infrared radiance. The deviations of computation and calculation are -10 per cent and 7.8 per cent, respectively. It can also be seen that, when the environmental radiation is not considered, there is an obvious deviation between the calculated data and measured data.

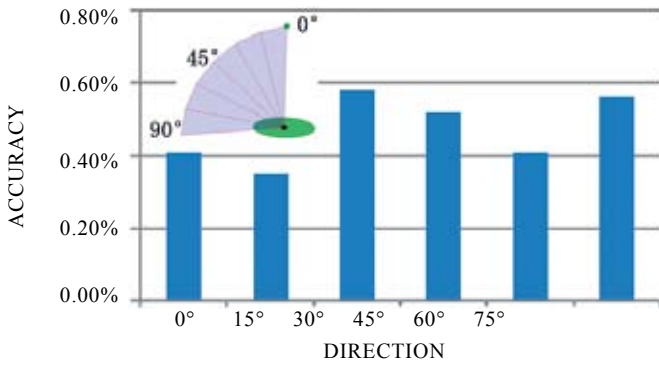


Figure 5. Comparison of computational results and theory results.

Table 1. Comparison with the calculated apparent infrared radiance and the measured apparent infrared radiance

	Paint	Foil
Measurement ¹⁴	37	23
Computation (self IR)	30.8	16.4
Computation (total)	33.3	24.8
Deviation	-10.0%	7.8%

When considering the environmental radiation, the deviation is evidently reduced. It should be noted that the environment IR radiation is very complex, and it is difficult to guarantee that the computation model is competent to all the real situations.

4. COMPUTATION EXAMPLE OF AN AIRCRAFT MODEL

4.1 Computation Conditions

Assume the flight altitude is 11 km, and speed is Mach 0.8. The composition of the mid-latitude summer and the mid-latitude winter atmosphere is used in the computation. The local temperature and pressure at the height of 11 km is 21990 pa and 228.2 K in summer; the local temperature and pressure at the height of 11 km is 24300 pa and 219.2 K in winter. Due to aerodynamic heating, the skin temperature will rise. The emissivity of the aircraft is 0.87.

A turbofan engine with bypass 3.5 is assembled in the aircraft. Table 2 shows the parameters of the turbofan engine.

The temperature of skin and engine cavity walls, the temperature field and species field of the plume were computed by using CFD code. These data is input data of infrared radiation computation. Figure 6 shows the distribution of the skin static temperature. The average temperature of the aircraft skin in the summer and winter is 256.4 K and 245.8 K, respectively.

Table 2. Parameters of the turbofan engine

Season	$p^*(pa)$	$T^*(K)$	Mole fractions	
			CO_2	H_2O
Summer	56770	873	0.045	0.047
	58310	305	0.00033	0.0
Winter	60290	837	0.042	0.046
	61760	286	0.00033	0.0

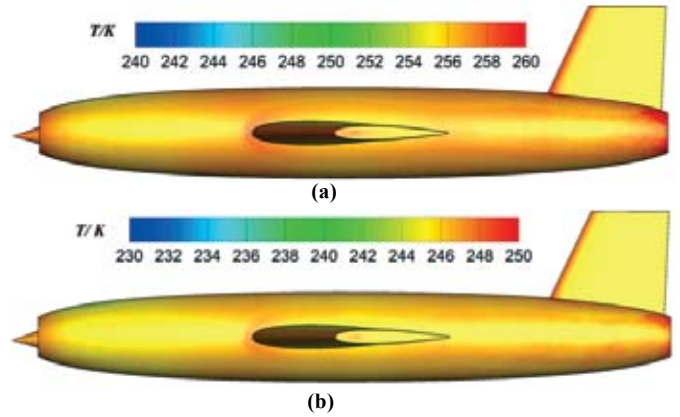


Figure 6. Distribution of the skin static temperature (units: K): (a) summer and (b) winter.

4.2 Results and discussion

4.2.1 Distribution of Self IR

The composition of aircraft self IR in long wave band is shown in Fig. 7. In the detection range of $\alpha = 0^\circ \sim 155^\circ$, the dominant contributor is aircraft skin, which emits 60% ~ 99% of the self IR. In the detection range of $\alpha = 155^\circ \sim 180^\circ$, the dominant contributor is engine hot walls. The contribution of plume is about 6 per cent on the rear side.

Comparison of self IR at different seasons is shown in Fig. 8. The aircraft self IR in summer is about 23 per cent larger than that in winter. The main reason is that the heating temperature in summer is higher.

The comparison of infrared radiance of the aircraft and the environmental radiance is shown in Fig. 9. It can be seen that the infrared radiance of the aircraft with flight speed Mach 0.8 at altitude 11 km is far greater than the background radiance when looking from aircraft to the top of atmosphere. However, the infrared radiance of the aircraft is far less than

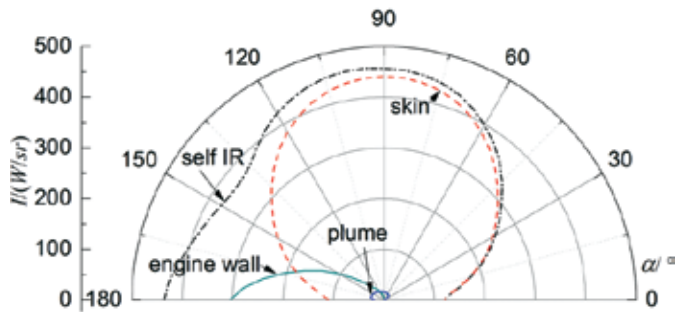


Figure 7. Composition of aircraft self IR in long wave band ($\beta=0^\circ$).

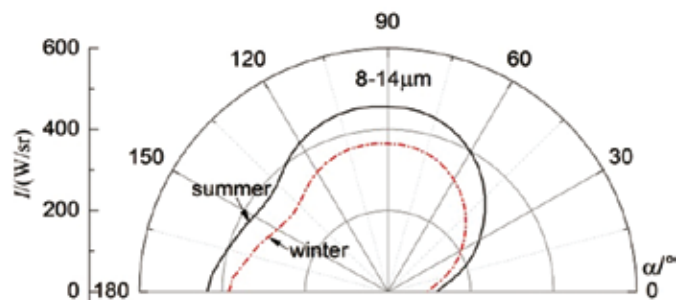


Figure 8. Comparison of self IR at different seasons ($\beta=0^\circ$).

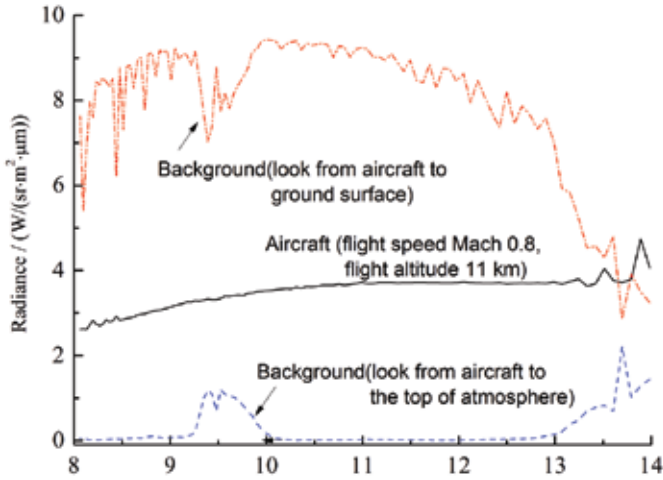


Figure 9. Comparison of infrared radiance of the aircraft and the environmental radiance.

the background radiance when looking from aircraft to the ground surface.

4.2.2 Distribution of Reflected IR

The distribution of the ratio of reflected IR to self IR is as shown in Fig. 10. The ratio values distributed in the front and side of the aircraft are bigger than that in the rear. The maximum ratio values is in the upward view plane ($\beta = -10^\circ$), and the minimum values is in the downward view plane ($\beta = 10^\circ$). The effect of background infrared radiation in summer is more obviously than that in winter at the same view angle. In summer, the average ratio of reflected IR to self IR is 12% in upward view plane, 9% in horizontal plane and 4.5% in downward view plane. In winter, the average ratio of reflected IR to self IR is 10%, 7.5%, and 3.5%, respectively.

4.2.3 Distribution of Thermal Figure

The thermal figure (7.7 μm - 14 μm) of aircraft at altitude of 11 km in summer is as shown in Fig. 11. Since the radiance of the atmosphere under the aircraft is much higher than that above the aircraft, and the existence of ground infrared, the apparent radiance temperature (in K) of the lower part of the aircraft is higher than that of upper part of the aircraft. The difference of radiance temperature between lower and upper surface of the aircraft is about 9 K. The nozzle seems to be a hot spot in the figure viewing from the rear side ($\alpha=165^\circ$, $\beta=-2^\circ$). The radiance temperature of nozzle is far higher than that of airframe. The distribution of thermal figure in winter is similar to summer, but the difference of radiance temperature between lower and upper surface of the aircraft is reduced to about 6 K.

5. CONCLUSIONS

The temperature and pressure in different seasons have different values, result in the aircraft self IR in summer is about 20 per cent larger than that in winter. The total infrared radiation will be increased by reflecting the background radiation. Typically, in the horizontal detection plane, the ratio of reflected background IR to the self IR is about 10 per cent in summer, and 7 per cent in winter. The distribution of the

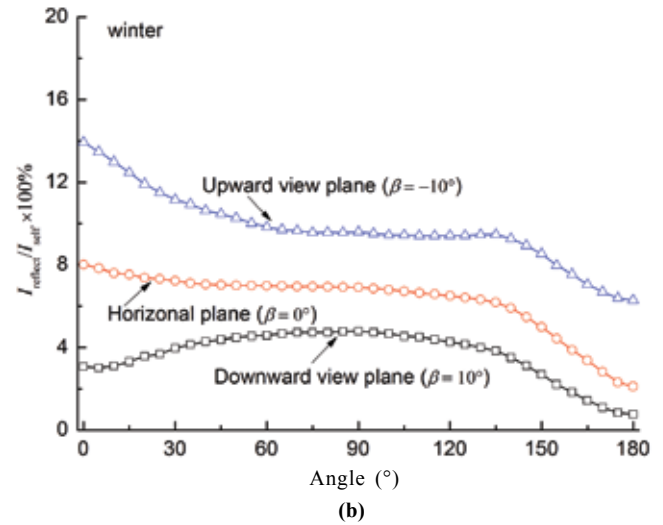
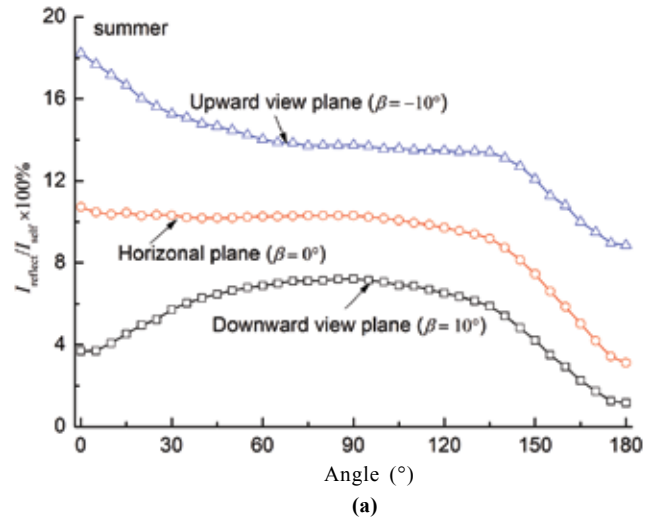


Figure 10. The ratio of reflected IR to self IR: (a) Summer and (b) Winter.

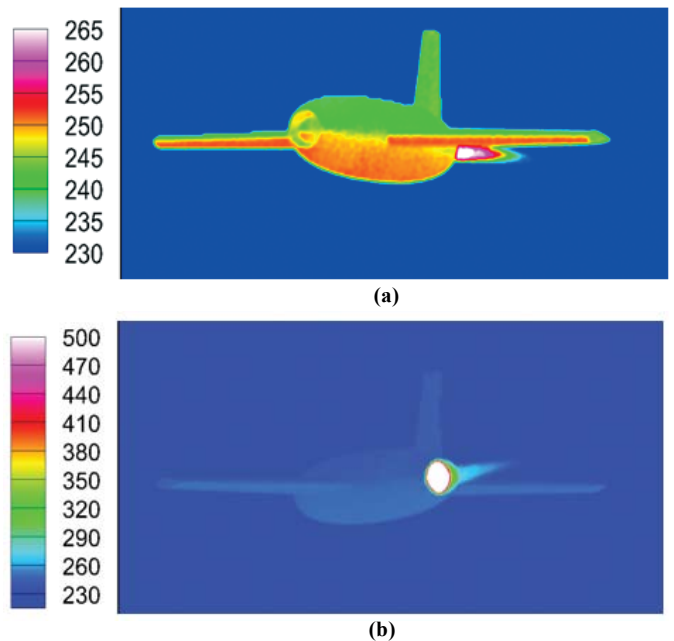


Figure 11. Thermal figures (7.7-14 μm) of aircraft at altitude 11 km in summer: (a) $\alpha=15^\circ$, $\beta=-2^\circ$; (b) $\alpha=165^\circ$, $\beta=-2^\circ$.

ratio of reflected IR to self IR in different detection plane is different. The ratio in upward detection plane has a bigger value than horizontal plane and downward detection plane. For the aircraft flying at altitude 11 km with speed Mach 0.8, the existence of atmospheric and ground IR makes the radiance temperature of the lower part of the aircraft 6 K (winter) ~ 9 K (summer) higher than that of the upper part of the aircraft. The temperature difference may be different with the change of flight speed, surface condition and environment. There has been a special concern for the application of low emissivity paints to reduce the aircraft IR, since the lower the emissivity, the higher the reflected IR.

REFERENCES

1. Renuka, D.V. & Reddy, K.M. Infrared background and missiles signature survey. *Def. Sci. J.*, 2013, **63**(6), 611-615.
doi: 10.14429/dsj.63.5762
2. Coiro, E. Global illumination technique for aircraft infrared signature calculations. *J. Aircraft*, 2013, **50**(1), 103-113.
doi: 10.2514/1.C031787
3. Mahulikar, S.P.; Sonawane, H.R. & Rao, G.A. Infrared signature studies of aerospace vehicles. *Progress Aerospace Sci.*, 2007, **43**(7-8), 218-245.
doi: 10.1016/j.paerosci.2007.06.002
4. Noah, M.; Kristl, J.; Schroeder, J. & Sandford, B.P. NIRATAM-NATO infrared air target model. *In Proceedings of SPIE*, 1991, **1479**, pp. 275-282.
doi: 10.1117/12.44537
5. Miller, R. EO/IR modeling of a generic aircraft (U). *In Proceedings of SPIE*, 1993, **1969**, pp. 150-156.
6. Bishop, G.J.; Caola, M.J.; Geatches, R.M. & Roberts, N.C. SIRUS spectral signature analysis code. *In Proceedings of SPIE*, 2003, **5075**, pp. 259-269.
doi: 10.1117/12.487716
7. Johansson, M. & Dalenbring, M. SIGGE, a prediction tool for aeronautical IR signatures, and its applications. 2006. AIAA 2006-3276.
doi: 10.2514/6.2006-3276
8. Johansson, M. & Dalenbring, M. Calculation of IR signatures from airborne vehicles. *In Proceedings of SPIE*, 2006, **6228**, pp. 622813-1-12.
doi: 10.1117/12.660108
9. Harkiss, S.I. A study of bi-directional reflectance distribution functions and their effect on infrared signature models. 2007. AFIT/GE/ENP/07-01.
10. Coiro, E. & Chatelard, C. Experimental validation of an aircraft infrared signature code for commercial airliners. 2012. AIAA 2012-3190.
doi: 10.2514/6.2012-3190
11. Rao, G.A. & Mahulikar, S.P. Effect of atmospheric transmission and radiance on aircraft infrared signatures. *J. Aircraft*, 2005, **42**(4), 1046-1054.
doi: 10.2514/1.7515
12. Lu, J. & Wang, Q. Aircraft-skin infrared radiation characteristics modeling and analysis. *Chinese J. Aeronaut.*, 2009, **22**(5), 493-497.
doi: 10.1016/S1000-9361(08)60131-4
13. Huang, W. & Ji, H.-h. Investigation of a two-dimensional hot jet's infrared radiation using four different turbulence models. *Math.l Probl. Eng.*, 2014, **2014**, 1-12.
doi: 10.1155/2014/298186
14. Nelsson, C.; Hermansson, P.; Winzell, T. & Sjökvist, S. Benchmarking and validation of IR signature programs: Sensorvision, Cameo-SIM and RadThermIR. 2005. ADA457113.

ACKNOWLEDGEMENTS

This study was supported by the China Aeronautic Science Funding, No. 20132752039.

CONTRIBUTORS

Dr W Huang obtained his PhD from Nanjing University of Aeronautics and Astronautics, China. He is currently working in Nanjing University of Aeronautics and Astronautics. He is having expertise in computational and experimental investigation of flow and heat transfer of aircraft. He is working in the area of radiative heat transfer of aero-engine and aircraft, infrared stealth of aircraft.

Dr H-H Ji obtained his PhD from University of Manchester Institute of Science and Technology, U.K. He is currently working as an outstanding professor at College of Energy and Power Engineering, Nanjing University of Aeronautics and Astronautics, China. He is working in the area of heat and mass transfer of aero-engine, ice accretion on the inlet components of aircraft engine, sealing of aero-engine and infrared stealth of aircraft etc.